



# COMPUTATIONAL PROGRESSIVE FAILURE OF COMPOSITE STRUCTURES

T.E. Tay, F. Shen, G. Liu, H.E. Chua, V.B.C. Tan [T.E. Tay]: mpetayte@nus.edu.sg  
Dept of Mechanical Engineering, National University of Singapore

**Keywords:** *Progressive Failure, Damage, Element-Failure Method (EFM), SIFT*

## Abstract

*In this article, a novel element-failure method (EFM) is proposed for modeling the progressive failure of pin-loaded composite joints. The basic concept of EFM is that only the nodal forces are modified to reflect changes in the load-bearing capability of the damaged finite elements. Instead of the conventional contact algorithm, a more convenient method is provided using the EFM to solve the contact problem between the composite hole edge and pin surface. In conjunction with the Tsai-Wu (TW) failure theory and a more recent micromechanics-based strain invariant failure theory (SIFT), the EFM is used to predict damage initiation and propagation in composite laminates. Comparisons are also made with the more commonly used material property degradation method (MPDM). It has been shown that a good agreement between numerical predictions and experimental results can be obtained by SIFT-EFM for three typical failure modes of pin-loaded composite joints.*

## 1 Introduction

Fastened joints are commonly used for assembling structural components in aircraft industry, which form weak points in the structures. The anisotropy and inhomogeneity of composites make the prediction of the ultimate strength of fastened composite joints very difficult. Damage in fastened composite joints can initiate at an early loading stage due to the stress concentration at the hole and accumulate and propagate inside the composites as the external load increases, eventually leading to ultimate failure.

Depending on the relative dimensions of the laminate and bolt, there are in general three basic failure modes related to fastened composite joints:

net-tension, shear-out and bearing [1,2]. The ultimate strengths of the joints are related to the materials, lay-ups, joint configurations, as well as bolt material, washer size, etc. [3]. Progressive failure models have been used by several authors [4-12] for strength analysis of fastened composite joints. By combining failure criteria and the material property degradation method (MPDM), the progressive failure models can reasonably predict final failure modes and ultimate failure load. The MPDM assumes that a damaged material can be replaced by an equivalent material with degraded properties. However, the stiffness matrix of the composites needs to be reformulated and inverted after modifying material properties of damaged elements, which is a computationally intensive process. There is also a possibility that by reducing the material properties, the stiffness matrix of the damaged element becomes ill-conditioned and convergence to a solution is not assured.

In this article, a novel FE-based element-failure method (EFM) is proposed for the modeling of progressive failure of fastened composite joints. The basic concept of EFM is that only the nodal forces are modified to reflect changes in the load-bearing capability of the damaged elements. Because the stiffness matrix remains unaltered, there are no computational problems associated with the MPDM. Another consequence is that there should be savings in computational effort since no reformulation of the stiffness matrix with damage progression is involved; each change in the damage state is modeled by appropriately modifying the nodal forces only. A recently proposed micromechanics-based failure theory, strain invariant failure theory (SIFT) [13], is used together with the EFM to determine damage initiation and propagation. In combination with a simple nodal force modification scheme, the SIFT-EFM approach takes into account mechanisms that bridge micro- and macro-length scales. In order for comparison, failure analysis of fastened composite joints is also performed using the well-known Tsai-Wu failure theory and the

traditional material property degradation method (MPDM).

In fastened composite joint problems, contact between the composite hole edge and pin surface is important and contributes significantly to the failure process. It is also demonstrated in this article that EFM can be an alternative to conventional contact algorithms for solving this contact problem.

## 2 Damage modeling techniques

### 2.1 Concept of the EFM

The idea and assumption of EFM is that the effects of damage on the mechanical behavior can be essentially described by the effective nodal forces of a finite element (FE). It was first developed for dynamic fracture in metals [14], but the modified EFM was used for impact damage in fiber-reinforced composites [15], damage progression in quasi-statically loaded three point bend composite laminates [16] and ultimate strengths of open-hole tension composite laminates [17]. The manner by which these effects due to damage translate to the effective nodal forces will in general depend upon the damage evolution law appropriate to the local mode of damage experienced by the composite material, as well as the finite element formulation [18].

Fig. 1(a) shows an FE of an undamaged composite material, subjected to a set of internal nodal forces, which have been obtained from the FE solution. On the other hand, a piece of damaged composite material, perhaps containing microcracks, will have its load-bearing capacity reduced, very likely in a directionally and spatially dependent manner. If much of the damage consists of transverse matrix microcracks, it is reasonable to assume that the FE of the damaged material will have reduced load-bearing capacity in the direction transverse to the fibers (Fig. 1(b)). In conventional material property degradation schemes, this reduction is achieved by reducing or zeroing certain pertinent material stiffness properties of the damaged finite element. In the EFM however, the reduction is effected by applying a set of external nodal forces such that the nett internal nodal forces of elements adjacent to the damaged element are reduced or zeroed (the latter if complete failure or fracture is implied (Fig. 1(c))). The decision whether to fail an element is guided by a suitable failure theory and in each step. The required set of applied nodal forces to achieve the reduction within each

step is determined by successive iterations until the nett internal nodal forces (residuals) of the adjacent elements converge to the desired values. Note that it is not the internal nodal forces of the damaged element that is zeroed (for the case of complete failure (Fig. 1(c))), but the nett internal nodal forces of adjacent elements. The EFM leaves the original (undamaged) material stiffness properties unchanged, and is thus computationally efficient since each iteration is simply an analysis with an updated set of applied nodal forces. Hence, no reformulation of the FE stiffness matrix is necessary.

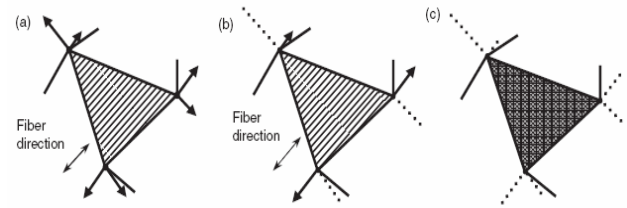


Fig. 1. (a) FE of undamaged composite with internal nodal forces.  
 (b) FE of composite with transverse matrix cracks. Components of internal nodal forces transverse to fiber direction are modified.  
 (c) Completely failed or fractured element. All net internal nodal forces of adjacent elements are zeroed.

### 2.2 The Material Property Degradation Method (MPDM)

In addition to the EFM, the material property degradation method (MPDM) is also used in this article for comparison. The assumption of the MPDM is that a damaged material can be replaced by an equivalent material with degraded properties. The effect of damage on material property degradation can be represented by internal state variables  $D_i^T$  and  $D_i^C$  which are function of the damage type:

for matrix tensile failure,

$$\begin{aligned} E_2^d &= D_2^T E_2 \\ G_{12}^d &= D_4^T G_{12} \\ G_{23}^d &= D_4^T G_{23} \end{aligned} \quad (1)$$

for matrix compressive failure,

$$\begin{aligned}
E_2^d &= D_2^C E_2 \\
G_{12}^d &= D_4^C G_{12} \\
G_{23}^d &= D_4^C G_{23}
\end{aligned} \quad (2)$$

for fiber tensile failure,

$$\begin{aligned}
E_1^d &= D_1^T E_1 \\
E_2^d &= D_2^T E_2 \\
G_{12}^d &= D_4^T G_{12} \\
G_{23}^d &= D_4^T G_{23}
\end{aligned} \quad (3)$$

for fiber compressive failure,

$$\begin{aligned}
E_1^d &= D_1^C E_1 \\
E_2^d &= D_2^C E_2 \\
G_{12}^d &= D_4^C G_{12} \\
G_{23}^d &= D_4^C G_{23}
\end{aligned} \quad (4)$$

where the superscript  $d$  denotes degraded material properties, the superscripts  $T$  and  $C$  represent tension and compression, respectively. The values of internal state variables are obtained from Camanho & Matthews [10]:  $D_1^T = 0.07$ ,  $D_2^T = D_4^T = 0.2$ ,  $D_1^C = 0.14$ ,  $D_2^C = D_4^C = 0.4$ .

### 3 Failure Criteria

#### 3.1 The Strain Invariant Failure Theory (SIFT)

A very brief description of the strain invariant failure theory (SIFT) is given here. SIFT is chosen because it is fully three-dimensional and it incorporates micromechanical features. Proposed by Gosse et al. [13], the theory determines if failure has occurred by considering the criticality of three strain invariant values, which have been ‘‘amplified’’ through micromechanical analysis. The strain components from homogenous FE solutions are amplified with thermo-mechanical amplification factors extracted from unit cell micromechanical FE models, before the invariants are calculated. The first strain invariant is  $J_1$ , defined by

$$J_1 = \varepsilon_{xx} + \varepsilon_{yy} + \varepsilon_{zz} \quad (5)$$

and the second deviatoric strain invariant  $J_2'$  is defined by

$$J_2' = \frac{1}{6} [(\varepsilon_{xx} - \varepsilon_{yy})^2 + (\varepsilon_{yy} - \varepsilon_{zz})^2 + (\varepsilon_{xx} - \varepsilon_{zz})^2] + (\varepsilon_{xy}^2 + \varepsilon_{yz}^2 + \varepsilon_{xz}^2) \quad (6)$$

where  $\varepsilon_{xx}$ ,  $\varepsilon_{yy}$ ,  $\varepsilon_{zz}$ ,  $\varepsilon_{xy}$ ,  $\varepsilon_{yz}$ , and  $\varepsilon_{xz}$  are the six components of the strain vector in general Cartesian coordinates. SIFT employs the von Mises (or equivalent) strain, which is related to the second deviatoric strain invariant by

$$\varepsilon_{vm} = \sqrt{3J_2'} \quad (7)$$

These strain invariants are amplified through the use of representative micromechanical blocks, whereby individual fiber and matrix are modeled by 3-D finite elements (Fig. 2). Three fiber arrangements or arrays are considered: square, hexagonal, and diamond. The diamond arrangement is in fact the same as the square, but rotated through a 45° angle. These representative micromechanical blocks are given prescribed unit displacements in three cases of normal and three cases of shear deformations in order to obtain strain amplification factors [16]. The local micromechanical strains are extracted from various positions within the model and normalized with respect to the prescribed strain. In addition to the above mechanical amplification factors, the so-called thermo-mechanical amplification factors may be obtained by constraining all the faces from expansion and performing a thermo-mechanical analysis by prescribing a unit temperature differential above the strain-free temperature.

Twelve locations are chosen for the extraction of local amplification factors for each micromechanical block. The points F1 through F8 are located at the fiber–matrix interface, F9 is located at the center of the (assumed circular) fiber, IF1 and IF2 are inter-fiber positions, and IS corresponds to the interstitial position. It is important to note that for a given matrix and fiber material system, the suite of micromechanical block analyses need only be performed once; the resulting amplification factors are stored in a look-up table or subroutine. The output of strains from a macro-FE analysis is efficiently amplified through this look-up subroutine before the strain invariant values are calculated and compared with the corresponding critical values. The amplification factors for carbon fiber–epoxy system used in all the analyses reported in this article were obtained from Gosse et al. [13], and coded in a look-up subroutine. However, the amplification factors have been independently verified by the authors, who performed the micromechanical FE block analyses. The matrix

(977-3) material properties were:  $E_m=3.31\text{GPa}$ ,  $\nu_m=0.35$ , while the fiber (IM7) was assigned transversely isotropic properties:  $E_f=303\text{GPa}$ ,  $E_{f2}=15.2\text{GPa}$ ,  $G_{f12}=9.65\text{GPa}$ ,  $G_{f23}=6.32\text{GPa}$ ,  $\nu_{12}=0.2$  and  $\nu_{23}=0.2$ . The subscripts  $m$  and  $f$  refer to matrix and fiber, respectively; the subscript 1 indicates the axial fiber direction, the subscripts 2 and 3 the transverse directions. These constituent material properties were obtained from Ha [19].

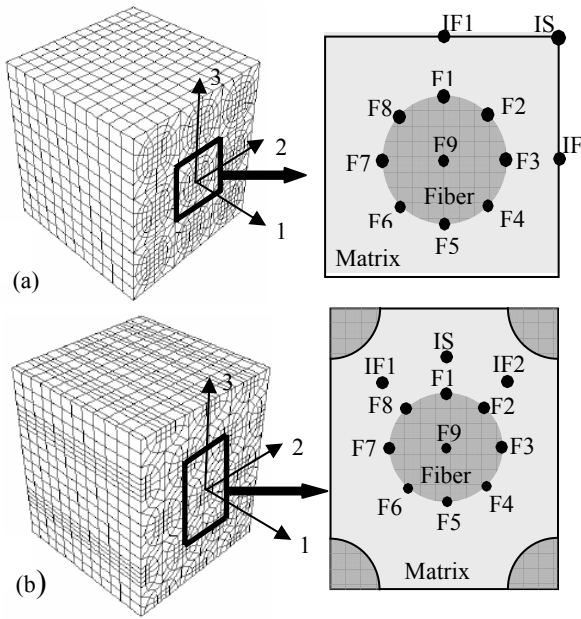


Fig.2. Locations for the extraction of amplification factors within the micromechanical block models: (a) square array; (b) hexagonal array

The first strain invariant  $J_1$  (Eq. 5.) is calculated with strains amplified only at the IF1, IF2, and IS positions within the matrix material in the micromechanical block. It is generally believed that  $J_1$ -driven failure is dominated by volumetric changes in the matrix material. On the other hand, the von Mises strain (Eq. 7.) may be amplified with factors not only within the matrix material (IF1, IF2, and IS), but also the fiber and fiber–matrix interface (F1 through F9). We designate the superscript  $m$  for the former case to denote “matrix” (i.e.  $\varepsilon_{vm}^m$ ), and the superscript  $f$  for the latter case to denote “fiber” (i.e.  $\varepsilon_{vm}^f$ ). SIFT states that failure occurs when either of the three strain invariant values reaches its respective critical values (i.e.,  $J_{1Crit}$ ,  $\varepsilon_{vmCrit}^m$  and  $\varepsilon_{vmCrit}^f$ ), which are determined from the analysis of the coupon tests of the composite laminates with various lay-ups [13].

When an element fails by either  $J_1$  or  $\varepsilon_{vm}^m$ , “partial” failure consisting of predominantly matrix microcracks, is assumed to have occurred. This corresponds to the state of damage depicted in Fig. 1(b), where only nodal forces perpendicular to the fiber direction are modified. On the other hand, when an element fails by  $\varepsilon_{vm}^f$ , it is necessary to determine first the location of the critical site within the micromechanical block model (Fig. 2), where the critical value has been calculated. If the critical site is at any one of the eight locations at the fiber–matrix interface (i.e., F1 through F8), “partial” failure is also assumed (Fig. 1(b)). The rationale for assigning partial failure despite  $\varepsilon_{vm}^f$  going critical in these locations is that local interfacial failure (or debonding) between fiber and matrix could have occurred. However, if the critical location is found within the fiber itself (F9 in Fig. 2), then the element is assumed to have completely failed and the nodal forces both perpendicular and parallel to the fiber direction are zeroed. In the analysis of fastened joints described subsequently, the critical locations in the case of  $\varepsilon_{vm}^f$  have always occurred at the fiber–matrix interface (and not within the fiber), and so “partial” failure has invariably been used with SIFT. It is conceivable, however, that an undamaged or already partially failed element (with mainly matrix microcracks and/or fiber–matrix microdebonds), at some point in the load history, may fail completely (by local fiber failure). It is therefore necessary to develop a criterion to determine when one element may become completely failed. A very simple criterion is to use the failure strain of carbon fibers. If the longitudinal strain of an element is greater than the fiber tensile failure strain or smaller than the fiber compressive failure strain, then this element is deemed to be completely failed and loses its load-bearing capability in both fiber and transverse directions.

### 3.2 Tsai-Wu Criterion

The well-known Tsai-Wu failure criterion [20] represents the failure criterion as a general quadratic in the stresses, which can be expressed as:

$$F_i \sigma_i + F_{ij} \sigma_i \sigma_j \geq 1 \quad (8)$$

where  $F_i$  and  $F_{ij}$  ( $i, j=1, 2, \dots, 6$ ) are tensor quantities of strength parameters

$$\begin{aligned}
F_1 &= \frac{1}{X} - \frac{1}{X_C}; & F_{11} &= \frac{1}{XX_C} \\
F_2 &= \frac{1}{Y} - \frac{1}{Y_C}; & F_{22} &= \frac{1}{YY_C} \\
F_3 &= \frac{1}{Z} + \frac{1}{Z_C}; & F_{33} &= \frac{1}{ZZ_C} \\
F_{44} &= \frac{1}{s_{23}^2}; & F_{55} &= \frac{1}{s_{13}^2}; & F_{66} &= \frac{1}{s_{12}^2}
\end{aligned} \tag{9}$$

where  $X$  and  $X_C$  are the longitudinal tensile and compressive strengths,  $Y$ ,  $Y_C$  and  $Z$ ,  $Z_C$  the transverse and normal tensile and compressive strengths, and  $S_{12}$ ,  $S_{23}$  and  $S_{13}$  the shear strengths in the 1-2, 2-3 and 1-3 plane, respectively.

While the Tsai-Wu failure theory is easy to use and very popular, it is in general unable to distinguish fiber-dominated failure from matrix-dominated failure. In this article, we use a simple method to determine the failure modes. First the failure condition (Eq. 8.) must be satisfied. If  $\sigma_{11} \geq X$ , fiber tensile failure is assumed, but if  $\sigma_{11} \leq X_C$ , fiber compressive failure is assumed. Otherwise, matrix failure is assumed.

#### 4 Application of the EFM on Contact Problems of Pin-Loaded Joints with Isotropic Materials

To demonstrate the applicability of EFM on contact problems, an isotropic plate with a pin-loaded hole in the center is used for comparison between the conventional contact algorithm and the EFM. The conventional contact algorithm is implemented in commercial FE code, ABAQUS, and the EFM in our own code. The size of the plate is 60mm×60mm×0.5mm. The radius of the hole is 5mm and perfect-fit is assumed. Only half of the plate is modeled due to symmetry about the plane  $y=0$ . Fig.5 shows the mesh of the model. The model is constrained at the left edge and the center of the pin is fixed. Prescribed displacement in  $x$  direction is imposed on the right edge of the model with up to 0.1% nominal strain. Three-dimensional brick elements are used with only one element in the thickness direction. The materials for the plate and pin are assumed to be different (Table 1.). The plate material is aluminum. A much higher Young's modulus is used for the pin to simulate a nearly rigid pin.

Different from the conventional contact algorithm, no contact surface exists in the EFM model. To simulate this contact problem, a special

layer of interface elements, which connects the plate and the pin, is used. The contact mechanism between the plate and the pin allows the nodes connecting the plate and interface elements to slide in the tangential direction of the hole, while prohibits penetration of the nodes into the pin. To simulate this mechanism, the interface elements are all failed in the tangential direction to allow the sliding around the surface of the pin. Those interface elements under tension in radial direction are fully failed (in both radial and tangential directions), while those under compression in radial direction are only failed in tangential direction (partially failed). All of these interface elements are failed by the EFM.

Table 1: Material properties of the isotropic model

|                 | Young's modulus (GPa) | Poisson's ratio |
|-----------------|-----------------------|-----------------|
| Plate           | 70                    | 0.35            |
| Pin             | $2 \times 10^4$       | 0.3             |
| Contact element | 70                    | 0               |

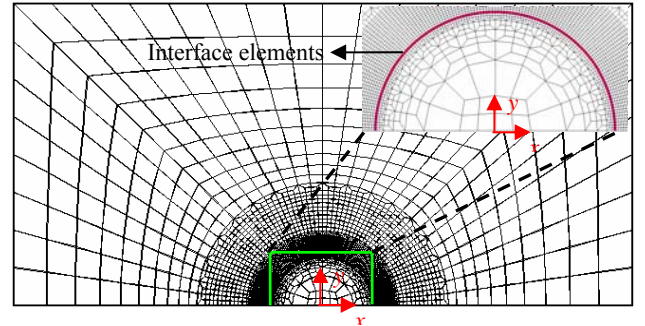


Fig. 3. Mesh of the isotropic model

Fig. 4 shows the comparison of displacements between the use of conventional contact algorithm and EFM. It can be seen that EFM gives nearly the same deformation as the conventional contact algorithm does. Figs. 5 and 6 show the distributions of strain  $\epsilon_x$  along the hole and mid-plane ( $x=0$ ) of the plate when the nominal strain is 0.1%. The results obtained by EFM agree very well with those by conventional contact algorithm. From these simulation results, it can be seen that using EFM, the contact problem between the plate and pin can be accurately simulated.

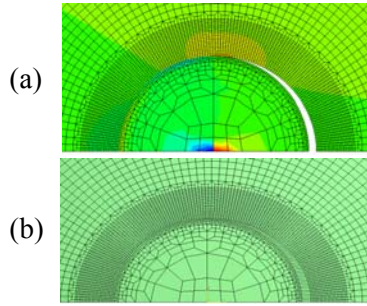


Fig. 4. Solution with (a) conventional contact algorithm, and (b) EFM, for a pin-loaded hole specimen.

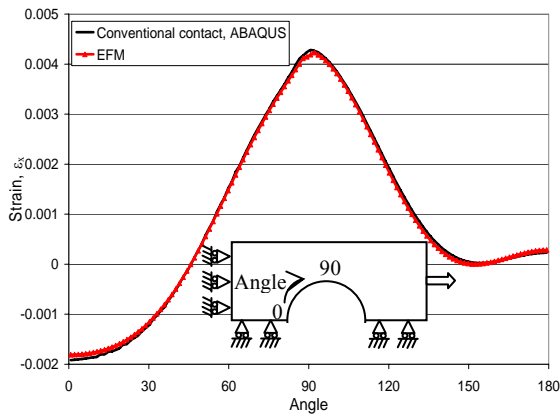


Fig. 5. Distribution of strain  $\epsilon_x$  around hole

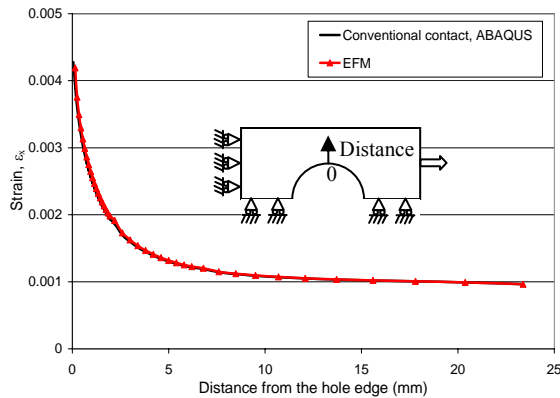


Fig. 6. Distribution of strain  $\epsilon_x$  along mid-plane

## 5 Failure Simulation on Pin-Loaded Composite Joints

The technique verified on the above isotropic model is applied to pin-loaded composite joints now. To verify the SIFT-EFM method, the simulation results are compared with published experimental observations.

### 5.1 Experimental specimens

Experimental results from Camanho & Matthews [10] are used for comparison. Dimensions of the specimens for three failure modes are given in Table 2 and Fig. 7. For all cases, the nominal thickness of the specimens is 2mm and the diameter  $D$  of the hole is 6mm. The specimens were made of T300/914 with a  $[0/90/45/-45]_{2s}$  lay-up. The composite material properties are given in Table 3.

Table 2: Dimensions of specimens (from Camanho & Matthews [10])

| Case        | W/D | E/D | L (mm) |
|-------------|-----|-----|--------|
| Bearing     | 6   | 6   | 100    |
| Net tension | 3   | 6   | 100    |
| Shear-out   | 6   | 1.5 | 100    |

Table 3: Material properties of T300/914 (from Camanho & Matthews [10])

|   |      |
|---|------|
| Modulus in fiber direction $E_1$ (GPa)            | 129  |
| Transverse moduli $E_2 = E_3$ (GPa)               | 9.5  |
| Shear moduli $G_{12} = G_{13}$ (GPa)              | 4.7  |
| Shear modulus $G_{23}$ (GPa)                      | 3.2  |
| Poisson's ratios $\nu_{12} = \nu_{13}$            | 0.34 |
| Poisson's ratio $\nu_{23}$                        | 0.52 |
| Longitudinal tensile strength $X$ (MPa)           | 1439 |
| Longitudinal compressive strength $X_C$ (MPa)     | 1318 |
| Transverse tensile strength $Y = Z$ (MPa)         | 98   |
| Transverse compressive strength $Y_C = Z_C$ (MPa) | 125  |
| Shear strength $S_{12} = S_{13} = S_{23}$ (MPa)   | 79   |

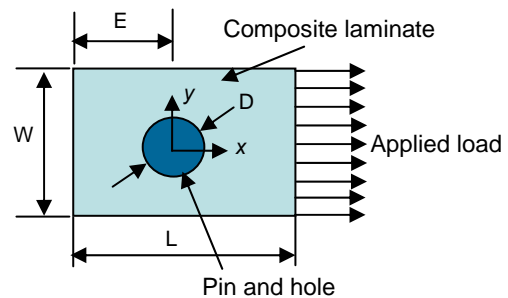


Fig. 7. Pin-loaded hole specimen

### 5.2 Numerical simulation

Finite element models are created based on the experimental specimens. 8-node brick elements are used and there is only one element in thickness direction for each ply.

The contact between the composite laminate and pin is simulated by using a circle of interface

elements around the hole. Here the pin is not explicitly modeled, and instead, the nodes on the hole surface are fixed to simulate a rigid pin. A prescribed displacement is imposed on the right edge of the models. Symmetric boundary conditions are imposed on the plane  $z=0$  because the lay-up is symmetric. The meshes used are shown in Fig. 8.

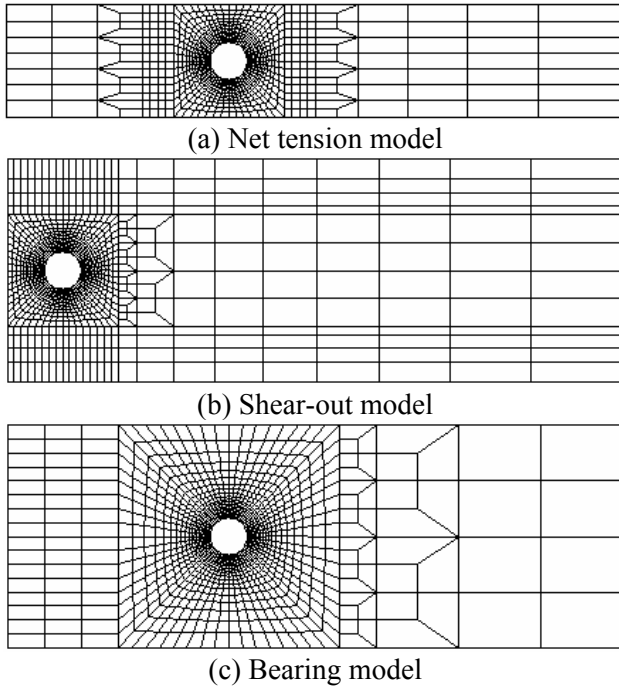


Fig. 9. Meshes for different failure mode models

### 5.2.1 Critical SIFT values

The critical SIFT values for T300/914 are not known. In Refs [16-18], we had used the values for IM7/977-3. Since the strengths of T300/914 are about 35%-50% lower than those of IM7/977-3, it is therefore assumed that all the critical values ( $J_1$ ,  $\varepsilon_{vm}^m$  and  $\varepsilon_{vm}^f$ ) for T300/914 are 40% lower than the critical values for IM7/977-3. The SIFT critical values used in the simulation are  $J_{1Crit}=0.0164$ ,  $\varepsilon_{vmCrit}^m=0.0618$  and  $\varepsilon_{vmCrit}^f=0.0109$ . In order to predict the fiber breakage, tensile and compressive failure strains of carbon fibers are also needed. The tensile failure strain of carbon fibers  $\varepsilon_{11}^t=0.016$  was taken as the tensile strength divided by the longitudinal modulus. The material properties of T300 were obtained from Herakovich [21]. Because no compressive strength or failure strain of carbon fibers is available in open literatures, an arbitrary value for the compressive failure strain  $\varepsilon_{11}^c=0.01$  is used in this analysis.

### 5.2.2 Assumption of residual strength for elements failed under local compression

In view of the experimental configuration (finger-tight washers were placed between the specimen and the pins, which formed constraint to the specimen), it is reasonable to assume that the elements failed due to local compression still have a certain percentage of load-carrying capability so that these elements can transfer some of the load to the neighboring unfailed elements. This is achieved by introducing internal state variables to degrade material properties of failed elements in Camanho & Matthews's work [10]. In this EFM analysis, a percentage of the internal nodal forces of neighboring unfailed elements are retained to represent the residual load-carrying capability of failed elements. Residual strength coefficients are introduced for this purpose. When EFM is applied to failed elements due to local compression, the residual nodal forces of neighboring unfailed elements will be the product of their original internal nodal forces and residual strength coefficients. The values of residual strength coefficients are the same as those of internal state variables in Ref [10]. For compressive fiber failure, the residual strength coefficient is assumed to be 0.14, and for compressive matrix failure, the residual strength coefficient is assumed to be 0.4. For those elements failed due to tension, the appropriate nodal forces are zeroed, which assumes that the failed elements have completely lost their load-bearing capability in the corresponding tensile direction.

### 5.2.3 Simulation results

#### 5.2.3.1 Strength prediction

The load-displacement curves by the SIFT-EFM, Tsai-Wu-EFM and Tsai-Wu-MPDM for all three cases are shown in Figs. 10-12. SIFT-EFM simulations agree very well with the experimental results before major load drop-off happens for the net tension and shear-out models. It will be seen in next subsection that major load drop-offs happen for these two models because damage has been extended to the laminate's free-edge (Figs. 13-14). For the bearing model, the load keeps increasing and a major load drop-off happens at an extremely large prescribed displacement. One possible reason is that the damage area is small and the failed elements due to local compression still have some load-bearing capability based on our assumption. However, this assumption of residual load-bearing capability is necessary in order to transfer load from the pin to the unfailed elements. Although the load keeps

increasing for large prescribed displacements for the bearing model, the turning point from linear to nonlinear part of the load-displacement curve is quite close to the experimental result.

Compared with the SIFT-EFM results, major load drop-offs happen at much smaller prescribed displacements for the Tsai-Wu-EFM (Figs. 10-12). Conservative ultimate strengths can be observed for the net tension and shear-out model, and overestimated ultimate strength for the bearing model. The load-displacement curves given by the Tsai-Wu-MPDM are very close to the SIFT-EFM results for these three failure mode cases, but there is no obvious load drop-off even loaded to a very large prescribed displacement.

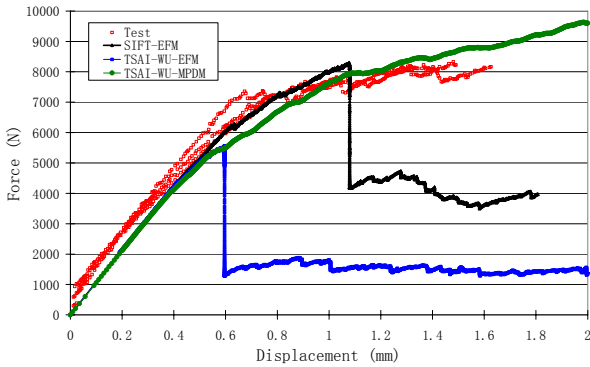


Fig. 10. Load-displacement curve (Net tension)

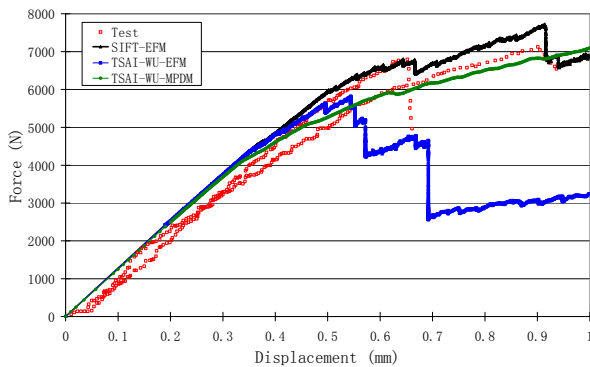


Fig. 11. Load-displacement curve (Shear-out)

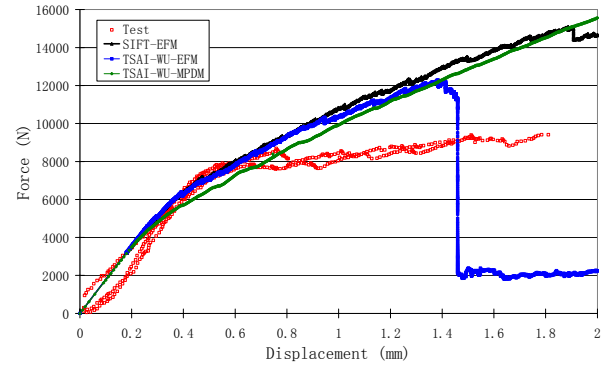


Fig. 12. Load-displacement curve (Bearing)

The experimental and SIFT-EFM predicted strengths are presented in Table 4. In the table, the experimental values are the maximum loads sustained by the joints [10]. The predicted strengths were obtained based on the same final failure criteria as Camanho & Matthews [10] used. For the net tension and shear-out models, the first load drop-off corresponds to the failure load. For the bearing model, the load at which the fiber failure reaches the edge of the washer (with an external diameter 12mm) is taken as the ultimate load. It can be seen that the errors between the experimental and predicted strengths are within 4% for all three cases.

Table 4: Predicted and experimental strengths

| Model       | Experimental (N) | SIFT-EFM (N) | Error |
|-------------|------------------|--------------|-------|
| Net tension | 8020             | 8300         | 3.5%  |
| Shear-out   | 6547             | 6780         | 3.6%  |
| Bearing     | 9803             | 10200        | 4.0%  |

### 5.2.3.2 Damage patterns

The comparisons between simulated and experimental damage patterns for all three cases are shown in Figs. 13-15. The predicted damage patterns are at the predicted failure loads described in 5.2.3.1. In the net tension model, matrix failure in the 90° plies is the initial failure mechanism. The fiber tensile failure along the laminate's width in the 0° plies causes the major load drop-off. In the shear-out model, matrix compressive failure is predicted in the 90°, 45° and -45° plies. The fiber compressive failure in the 0° plies contributed to the major load drop-off. At the final failure load, fiber failure has reached the end of the laminate. In the bearing model, the main failure mechanism is fiber compressive failure and it happens mainly in the bearing side of the hole. Because of the relatively small width ( $W$ ) for the net tension model and relatively small end distance ( $E$ ) for the shear-out model, damage is easily extended to the free edge of the laminate. But for the bearing

model, the damage is confined to a small area close to the hole surface because of the large width ( $W$ ) and end distance ( $E$ ). In general, the damage patterns are in good agreement with the experimental results for the three cases.

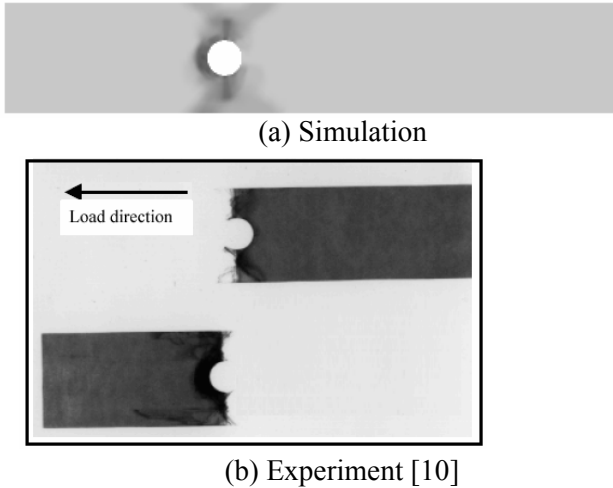


Fig. 13. Damage pattern (net tension)

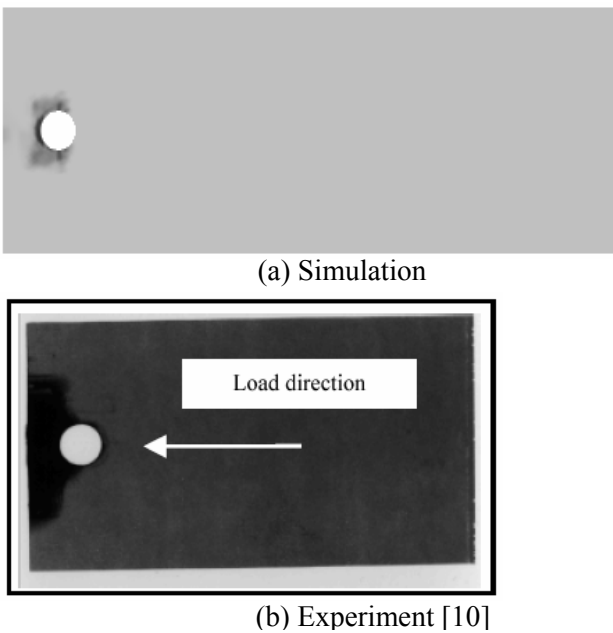


Fig. 14. Damage pattern (shear-out)

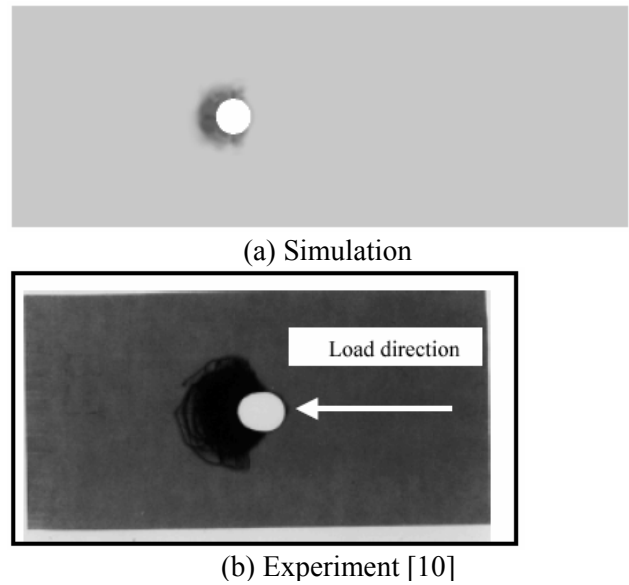


Fig. 15. Damage pattern (bearing)

## 6 Conclusions

The element-failure method (EFM) has been implemented in a three-dimensional implicit code to model the damage progression in pin-loaded composite joints. It assumes that the deleterious effects of damage on mechanical properties can be effectively achieved by modifying the nodal forces of failed finite elements. This leaves the original material properties unchanged, ensuring that no recalculation of stiffness matrices is necessary. The EFM also provides a convenient method to deal with contact problems. Different from the conventional contact algorithm, no contact surface is needed and only a circle of interface elements are failed by the EFM to model the contact condition. In conjunction with a micromechanics-based failure theory, strain invariant failure theory (SIFT), EFM is proved to be able to accurately predict the damage patterns and ultimate strengths for three failure modes of pin-loaded composite joints: net tension, shear-out and bearing.

## References

- [1] Camanho PP. and Matthews FL. "Stress analysis and strength prediction of mechanically fastened joints in FRP: a review". *Composites: Part A*, Vol. 28A, pp 529-547, 1997.
- [2] Camanho PP., Bowron S. and Matthews FL. "Failure mechanisms in bolted CFRP". *J. Reinforced Plastics and Compos*, Vol. 17, No. 3, pp 205-233, 1998.
- [3] Collings TA. "Experimentally determined strength of mechanically fastened joints". In: *Matthews FL.(ed)*,

- editor, *Joining fibre-reinforced plastics*, London: Elsevier Applied Science, pp 9-64, 1987.
- [4] Chang FK. and Chang KY. "Post-failure analysis of bolted composite joints in tension or shear-out model failure". *J Compos Mater*, Vol. 21, pp 809-833, 1987.
- [5] Lessard LB. and Shokrieh MM. "Two-dimensional modeling of composite pinned-joint failure". *J Compos Mater*, Vol. 29, No. 5, pp 671-696, 1995.
- [6] Hung CL. and Chang FK. "Bearing failure of bolted composite joints. Part II: model and verification". *J Compos Mater*, Vol. 30, No. 12, pp 1359-1400, 1996.
- [7] Dano ML., Gendron G. and Picard A. "Stress and failure analysis of mechanically fastened joints in composite laminates", *Compos Struct*, Vol. 50, pp 287-296, 2000.
- [8] Icten BM., and Karakuzu R. "Progressive failure analysis of pin-loaded carbon-epoxy woven composite plates". *Comp Sci Tech*, Vol. 62, pp 1259-1271, 2002.
- [9] Okutan B. "The effects of geometric parameters on the failure strength for pin-loaded multi-directional fiber-glass reinforce epoxy laminate". *Composites: Part B*, Vol. 33, pp 567-578, 2002.
- [10] Camanho PP. and Matthews FL. "A progressive damage model for mechanically fastened joints in composite laminates". *J Compos Mater*, Vol. 33, No. 24, pp 2249-2280, 1999.
- [11] McCarthy CT., McCarthy MA. and Lawlor VP. "Progressive damage analysis of multi-bolt composite joints with variable bolt-hole clearances". *Composites: Part B*, Vol. 36, pp 290-305, 2005.
- [12] Van Rooijen RGJ., Sinke J., De Vries TJ. and Van Der Zwaag S. "The bearing strength of fiber metal laminates". *J Compos Mater*, Vol. 40, No. 1, pp 5-19, 2006.
- [13] Gosse JH. and Christensen S. "Strain invariant failure criteria for polymers in composite materials". *AIAA-2001-1184*. 2001.
- [14] Beissel SR., Johnson GR. and Popelar CH. "An element-failure algorithm for dynamic crack propagation in general directions". *Eng Frac Mech*, Vol. 61, pp 407-425, 1998.
- [15] Tay TE., Tan VBC. and Deng M. "Element-failure concepts for dynamic fracture and delamination in low-velocity impact of composites". *Int J Solids and Struct*, Vol. 40, pp 555-571, 2003.
- [16] Tay TE., Tan SHN., Tan VBC. and Gosse JH. "Damage progression by the element-failure method (EFM) and strain invariant failure theory (SIFT)". *Comp Sci Tech*, Vol. 65, No. 6, pp 935-944, 2005.
- [17] Tay TE., Liu G. and Tan VBC. "Damage progression in open-hole tension laminates by the SIFT-EFM approach". *J Compos Mater*, Vol. 40, No. 11, pp 971-992, 2005.
- [18] Tay TE., Tan VBC. and Tan SHN. "Element-failure: an alternative to material property degradation method for progressive damage in composite structures". *J Compos Mater*, Vol. 39, No. 18, pp 1659-1675, 2005.
- [19] Ha SK. "Micromechanics in the analysis of composite structures". *6<sup>th</sup> Composite Durability Workshop (CDW-6)*, Tokyo, Japan, 14-15 November 2002.
- [20] Tsai SW. and Wu EM. "A general theory of strength for anisotropic materials". *J Compos Mater*, Vol. 5, pp 58-80, 1971.
- [21] Herakovich CT. *Mechanics of fibrous composite*, John Wiley & Sons, Inc., New York, 1998.